

Seismic behavior of unbonded post-tensioned precast concrete members with thin rubber layers at the jointed connection

Dimitrios Kalliontzis and Sri Sritharan

- This paper investigates the use of thin rubber layers to mitigate the seismic response of precast concrete members with jointed connections.
- An experimental investigation was undertaken using thin rubber layers at the interface between a precast concrete member and adjacent connection elements. Test variables included the shore hardness and thickness of the rubber.
- A single-degree-of-freedom model was verified using the experimental data of this research study and was employed to investigate the seismic response of precast concrete members with thin rubber layers.
- It was concluded that thin rubber layers with high shore hardness will effectively improve the damping capability of precast concrete members.

Figure 1 shows a precast concrete member with a jointed connection at the foundation base that uses unbonded post-tensioning, a concept that has been used for precast concrete structures for the past two decades.^{1–10} When subjected to lateral loads, the bottom corner of the member uplifts as it undergoes a rocking motion. During this motion, the member response is controlled by the axial force developed in the unbonded post-tensioning tendon, which recenters the member upon removal of the loads, concentrating inelastic deformations at its toes. With appropriate detailing of the toe region, the damage induced by rocking is minimal and the corresponding force-displacement response encloses little energy loss (that is, hysteretic energy dissipation). This energy loss is generally viewed as an inadequate means of dissipating the seismic energy imparted to the precast concrete member.

Apart from the hysteretic energy dissipation, precast concrete members with jointed connections dissipate additional energy during the dynamic impacts on the foundation base. Several research studies^{1–7} focused on the quasi-static behavior of these members, neglecting the impact energy loss. More recently, Nazari et al.⁸ and Kalliontzis et al.^{9,10} used shake table and free vibration tests, respectively, to investigate the impact energy loss. To achieve appropriate test conditions, the test specimens included no supplemental hysteresis elements (such as those used by Sritharan et al.⁶ and Twigden et al.⁷).

Using four precast concrete walls, Nazari et al.⁸ quantified the impact energy loss in terms of an equivalent viscous

PCI Journal (ISSN 0887-9672) V. 66, No. 1, January–February 2021.

PCI Journal is published bimonthly by the Precast/Prestressed Concrete Institute, 8770 W. Bryn Mawr Ave., Suite 1150, Chicago, IL 60631.

Copyright © 2021, Precast/Prestressed Concrete Institute. The Precast/Prestressed Concrete Institute is not responsible for statements made by authors of papers in *PCI Journal*. Original manuscripts and discussion on published papers are accepted on review in accordance with the Precast/Prestressed Concrete Institute's peer-review process. No payment is offered.

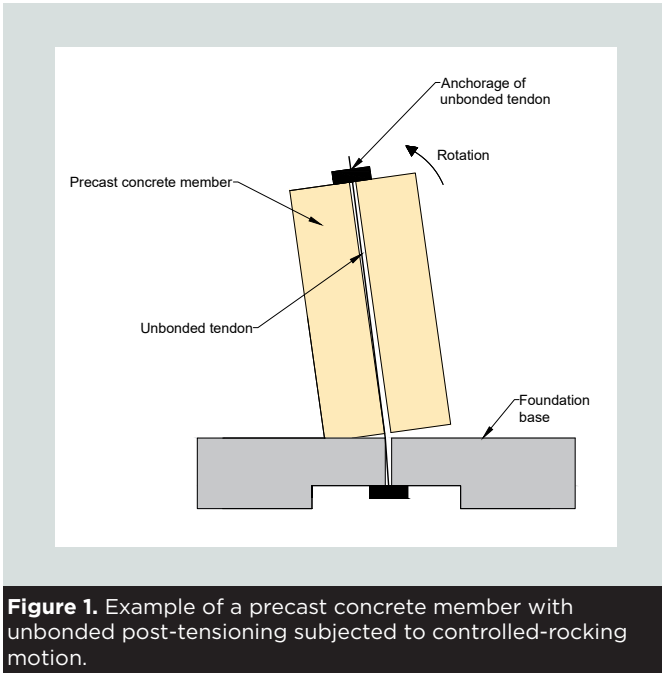


Figure 1. Example of a precast concrete member with unbonded post-tensioning subjected to controlled-rocking motion.

damping ratio ζ , attributing an average value of 1.5% to this ratio for single rocking walls. Despite the low damping produced by impacts, Nazari et al.⁸ observed that precast concrete walls can produce satisfactory seismic response when subjected to design-level earthquakes. Nevertheless, it was observed that when the walls are subjected to maximum considered earthquakes, their seismic response may exceed the permissible lateral displacements.

Using three precast concrete members representing columns and walls, Kalliontzis et al.⁹ quantified impact energy loss in terms of a coefficient of restitution r .¹¹ Accordingly, a generalized formula was developed, which assumes that the coefficient of restitution r is a function of the geometric properties of the precast concrete members and their pivot point locations just before and just after the impacts. A more recent study¹⁰ showed that the experimental measurements of impact energy loss by Nazari et al.⁸ agreed with the generalized formula.⁹ The same study¹⁰ corroborated that precast concrete members with jointed connections may undergo large lateral drifts when subjected to horizontal ground motions. As described in this paper, these large drifts may be attributed to the low damping in the precast concrete members, which may not exceed 5% of an equivalent viscous damping ratio ζ .

Research significance

This research study investigated the use of a method to improve the damping capability of precast concrete members by placing thin rubber layers at their jointed connections. Through this method, the intent was to improve the seismic behavior of these members so that they can be designed without supplemental hysteresis elements. For this purpose, free vibration tests of a precast concrete member were employed. The test variables were the class of the rubber in terms of shore hardness SH and the thickness of the rubber layers t_r .

An analytical investigation following these tests examined the effect of rubber layers on the behavior of precast concrete members with jointed connections. It was concluded that thin rubber layers with high shore hardness SH will effectively mitigate the members' seismic responses.

Formulation of energy losses

This section discusses the state of knowledge relevant to energy loss resulting from rocking response and recent improvements. The first steps toward understanding the seismic behavior of rocking members were undertaken by Housner,¹¹ who conducted an analysis of rigid, freestanding, planar rocking members without unbonded post-tensioning. The equation that governs the rotational motion of these bodies can be expressed in compact form as follows:

$$I_o \ddot{\theta} + MgR_0 \sin[\text{sign}(\theta)a - \theta] = -MR_0 \ddot{u}_g \cos[\text{sign}(\theta)a - \theta] \quad (1)$$

where

I_o = mass moment of inertia of the rocking member about its pivot point

$\ddot{\theta}$ = angular acceleration of the rocking member

M = total mass of the rocking member

g = acceleration due to gravity

R_0 = distance of pivot point from center of gravity of the rocking member

$\text{sign}(\theta)$ = sign of angular displacement

a = slenderness coefficient of the rocking member
 $= \tan^{-1} \left(\frac{\text{member base width}}{\text{member height}} \right)$

θ = angular displacement of the rocking member

\ddot{u}_g = horizontal ground acceleration

When the angular displacement of the rocking member with respect to the foundation base $\theta \rightarrow 0, \dots$ the rocking member impacts the foundation base, producing energy loss, which was quantified by Housner¹¹ in terms of the coefficient of restitution r :

$$r = \frac{K_2}{K_1} = \left[1 - \frac{3}{4}(1 - \cos(2a)) \right]^2 \quad (2)$$

where

K_1 = kinetic energy of the rocking member just before the impact event

K_2 = kinetic energy of the rocking member just after the impact event

Several researchers^{12–21} showed that Eq. (2) may overestimate the experimentally established impact energy loss. Kalliontzis et al.⁹ introduced an improved formula based on experiments of precast concrete members, including the jointed wall system tested in the PRESSS (Precast Seismic Structural Systems) building:²

$$r = \left[\frac{4 - 3(\sin a)^2(1 + k^2)}{4 - 3(\sin a)^2(1 - k^2)} \right]^2 \quad (3)$$

where

k = ratio of the distance between the pivot points just before and just after impact over the precast concrete member's base width

In the absence of available data, Kalliontzis et al.⁹ suggested a ratio of the distance between the pivot points just before and just after impact over the precast concrete member's base width k of 0.72. The use of a ratio of the distance between the pivot points just before and just after impact over the precast concrete member's base width k of 0.72 was shown later by Kalliontzis and Sritharan¹⁰ to provide good accuracy for precast concrete members with different geometries, material properties, and unbonded post-tensioning designs. For practical purposes, energy loss in precast concrete members can be expressed as an equivalent viscous damping ratio ζ . Priestley et al.¹² developed a formula for equivalent viscous damping ratio ζ to compute the total energy loss in rocking members subjected to free vibration motions. As defined by Priestley et al., equivalent viscous damping ratio ζ may include other energy losses (for example, due to friction or viscous damping) in addition to those produced by impact. The proposed expression for the equivalent viscous damping ratio ζ is detailed in Eq. (4):

$$\zeta = \frac{1}{\pi n} \ln \left(\frac{\theta_o}{\theta_n} \right) \quad (4)$$

where

n = number of impacts

θ_o = initial angular displacement of the free vibration motion

θ_n = amplitude of angular displacement after n impacts

Using Eq. (4) with a number of impacts n of 1, the computed equivalent viscous damping ratio ζ corresponds to a time duration of one-half rocking period, which includes one impact. When the number of impacts n equals 2, Eq. (4) becomes identical to the damping ratio estimation for linear-elastic single-degree-of-freedom (SDOF) oscillators.²²

More recently, another expression for equivalent viscous damping ratio ζ was presented by Makris and Konstantinidis,²³ assuming that equivalent viscous damping ratio ζ is only a function of the coefficient of restitution r , which im-

plies that all energy losses in rocking members occur during the impacts:

$$\zeta = -\beta \ln r \quad (5)$$

where

β = dimensionless modeling parameter

For infinitely rigid and freestanding rocking members, Eq. (5) with a dimensionless modeling parameter β of 0.34 and coefficient of restitution r per Eq. (2) (Housner's formula¹¹) was analytically shown by Makris and Konstantinidis²³ to accurately reproduce an equivalent viscous damping ratio ζ of Eq. (4). However, based on experimental measurements presented by Nazari et al.,⁸ it is suggested in this paper that a dimensionless modeling parameter β of 0.15 may be a more suitable value for the equivalent viscous damping ratio ζ of precast concrete members because of the deformations that these members experience at the rocking interface.

Figure 2 presents several estimates of the impact energy loss in terms of equivalent viscous damping ratio ζ based on previous experiments^{8–10,12–20,24,25} compared with the theoretical equivalent viscous damping ratio ζ of Eq. (5) with a dimensionless modeling parameter β of 0.15 and coefficient of restitution r per Eq. (3). For a given value of height-to-width ratio h/b , the equivalent viscous damping ratio ζ values can differ among the referenced experiments. For example, when the height-to-width ratio h/b equals 4, equivalent viscous damping ratio ζ varies from 0.93% to 3%, while similar deviations occur for a height-to-width ratio h/b of 2. As explained by Kalliontzis et al.,⁹ these variations can stem from imperfections at the jointed connection due to construction tolerances and the use of different materials in the experiments. Another explanation for these variations could be the use of different methods of experimentally establishing equivalent viscous damping ratio ζ . For practical purposes, the proposed theoretical model provides a reasonable correlation to the experimentally estimated values of equivalent viscous damping ratio ζ .

Another observation from Fig. 2 is that the height-to-width ratio h/b of vertical precast concrete members (that is, columns and walls) will be higher than 2.0, implying that the equivalent viscous damping ratio ζ will be less than 5%. This observation combined with the design code expectation²⁶ of a 12.5% damping ratio suggests that some additional damping will be needed in precast concrete members. For this reason, an experimental investigation was undertaken using rubber layers at the interfaces between these members and adjacent connection elements.

Experimental investigation

Test setup

A precast concrete member was tested in the structural laboratory of Iowa State University in Ames with free vibration excitations. Geometry, material properties, and

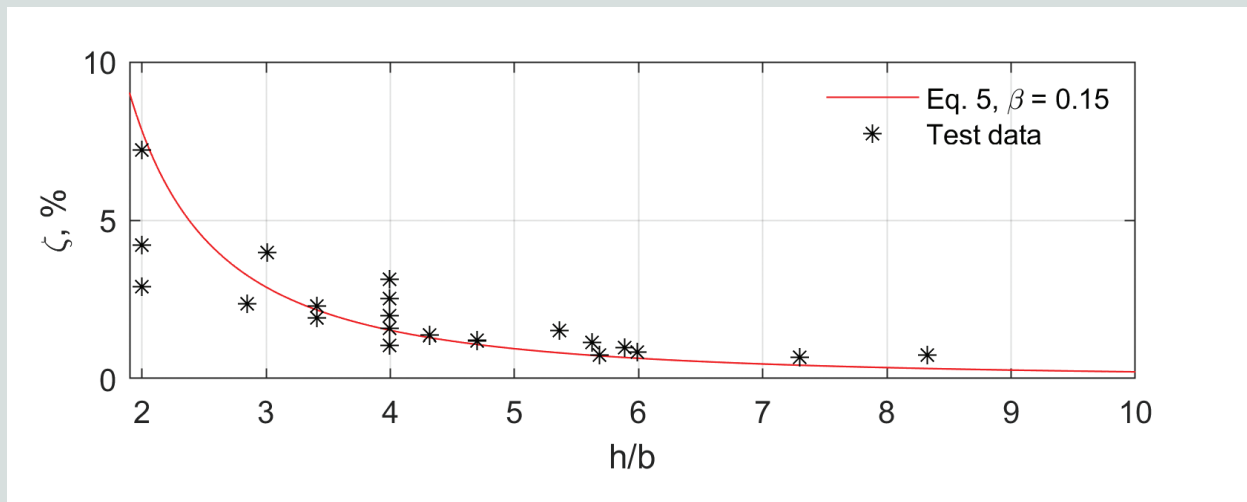


Figure 2. Experimentally measured and theoretical estimates of the equivalent viscous damping ratio ζ attributed to impact energy loss. Note: b = base width of precast concrete member; h = height of precast concrete member; β = dimensionless modeling parameter taken equal to 0.15.

reinforcement details of the member were defined to match the characteristics of precast concrete members designed for prototype buildings.^{2,6,8} The member was 177.8 mm (7 in.) deep \times 711.2 mm (28 in.) wide \times 2425.7 mm (95.5 in.) high and was tested on a concrete foundation that was 1270 mm (50 in.) deep \times 1270 mm wide \times 609.6 mm (24 in.) high.

To ensure full contact between the precast concrete member and the foundation surface, a 25.4 mm (1 in.) thick non-shrink grout layer was placed into a pocket on top of the foundation base. A neoprene rubber layer with thickness ranging from zero (that is, no rubber) to 25.4 mm was placed on the top of the grout layer prior to placing the precast concrete member. Damage to the member was minimized by placing steel angle members along the rocking edges and firmly embedding them in the member using 50 mm (1.97 in.) long shear studs. These steel elements prevented potential crushing of the cover concrete due to impacts. Reinforcement details of the precast concrete member are presented in Fig. 3.

Free vibration tests

An electric pump and a hydraulic jack were used to induce the lateral displacements at the top of the precast concrete member. A quick-release device was subsequently used to initiate the free vibration motions with initial top lateral drifts in the following order: 1%, 2%, and 3%. Each initial top lateral drift test was repeated three times.

Instrumentation

The instrumentation included a motion-tracking system with light-emitting diodes (LEDs) that were attached to the surface of the test unit as shown in Fig. 3. The experimen-

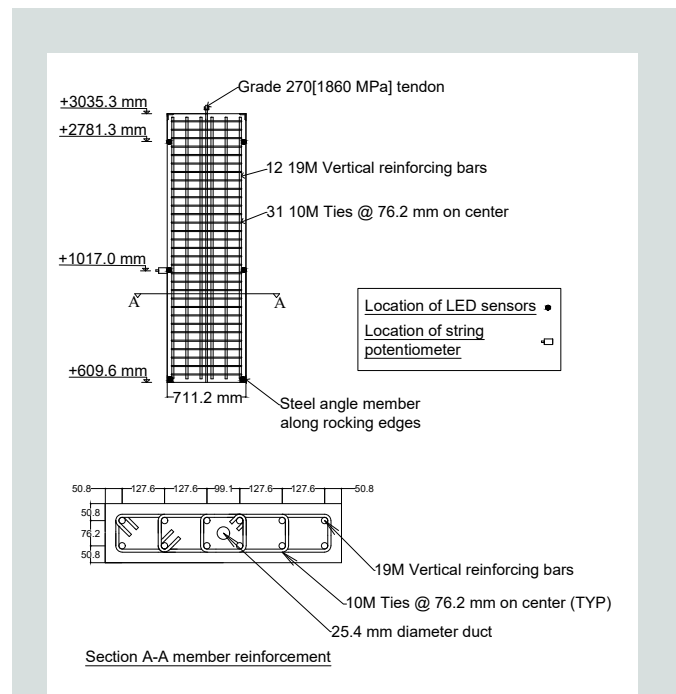


Figure 3. Reinforcement details of the test unit and locations of LED sensors and potentiometers. Note: All dimensions are expressed in millimeters. 10M = no. 3; 19M = no. 6; 1 mm = 0.0394 in.

tal data collected from the LEDs were used to compute the lateral displacement-versus-time histories of the precast concrete member relative to the foundation base. In addition, a string potentiometer was used to obtain independent measurements of the member's lateral movement as a function of time. A load cell was placed on top of the member to measure the post-tensioning force during the free vibration motions.

Table 1. Initial post-tensioning force as recorded by the load cell just before the tests

Test sequence	Material layer	Shore hardness <i>SH</i>	Thickness, mm	Initial post-tensioning force, kN
1	Grout	n/a	25.4	17.8
2	Rubber	50	6.35	16.9
3	Rubber	50	12.7	22.2
4	Rubber	50	25.4	20.0
5	Rubber	70	25.4	24.0
6	Rubber	90	25.4	26.9

Note: n/a = not applicable. 1 mm = 0.0394 in.; 1 kN = 0.225 kip.

Interface materials

As shown in **Table 1**, the precast concrete member was first tested using a grout layer at the jointed connection with a specified compressive strength of 70 MPa (10 ksi). The subsequent tests placed rubber layers on top of the existing grout layer. The rubber layers were not firmly attached to the member, allowing separation at the appropriate interfaces during the rocking motions. Three classes of neoprene rubber were used with a shore hardness *SH* of 50, 70, and 90. All rubber layers had sectional dimensions of 177.8 mm (7 in.) deep × 711.2 mm (28 in.) wide, matching the cross section of the member within a tolerance of 3 mm (0.12 in.). The rubber layers with a shore hardness *SH* of 70 and 90 had a thickness of 25.4 mm (1 in.). Three levels of thickness were used for the rubber layer with a shore hardness *SH* of 50: 25.4, 12.7, and 6.35 mm (1, 0.5, and 0.25 in.).

Unbonded post-tensioning

The precast concrete member was post-tensioned using Grade 270 (1860 MPa) unbonded seven-wire strand with a diameter of 15.24 mm (0.60 in.) and unbonded length of 2832.1 mm (111.5 in.). The target initial post-tensioning force was 30 kN (6.74 kip), selected to ensure that the strand responded elastically up to the lateral drift of 3%. Due to losses from anchorage slip, the initial post-tensioning forces were reduced upon removal of the hydraulic jack. Table 1 presents all values of the initial post-tensioning forces as recorded by the load cell just before the tests. No reduction to the initial post-tensioning forces was indicated by the load cell at the end of the tests.

Experimental results

This section presents the experimental responses of the six test systems detailed in Table 1. All test systems performed satisfactorily, which was indicated by the reproducible responses at each initial top lateral drift. Moreover, no damage was observed to the precast concrete member, the strands, interface material layers, or the foundation.

Time histories of lateral drift **Figure 4** presents experimentally measured time histories of lateral drift for all tests,

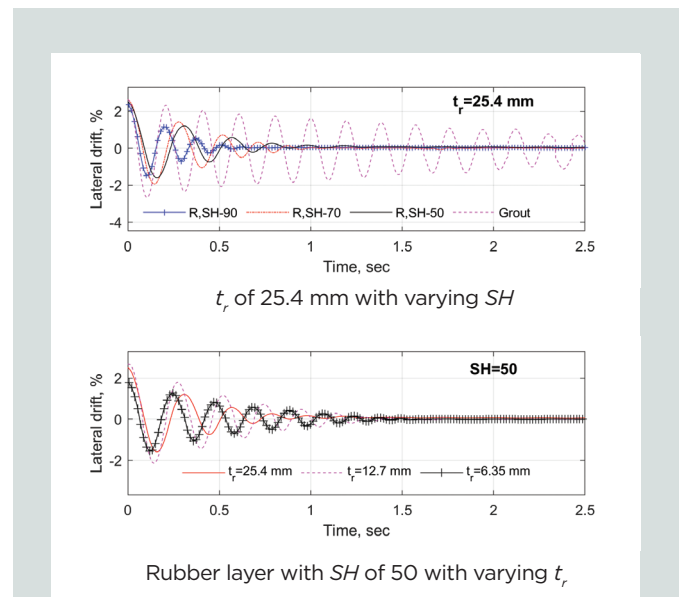


Figure 4. Time-histories of lateral drifts in test systems with rubber thickness t_r of 25.4 mm with varying shore hardness *SH* and a rubber layer with a shore hardness *SH* of 50 with varying rubber thickness t_r . Note: R = rubber. 1 mm = 0.0394 in.

with initial top lateral drifts near 2%. The top graph in Fig. 4 compares all test systems with an interface layer thickness of 25.4 mm (1 in.), showing that the responses with rubber decayed significantly faster than the test system with grout. For example, the drift amplitudes of the test systems with rubber approached zero after about 1.0 second from the beginning of the free vibration, while the test system with grout continued to oscillate for several more seconds. After 2.0 seconds, the drift amplitude of the test system with grout decreased to 50% of its initial value. The bottom graph in Fig. 4 compares the three lateral drift responses of the test systems with a rubber shore hardness *SH* of 50 and three different layer thicknesses: 25.4, 12.7, and 6.35 mm (1, 0.5, and 0.25 in.). It is generally shown that the use of these rubber layers also improved the decay of motion of the precast concrete member.

Equivalent viscous damping ratio The overall damping of the test systems was investigated using the corresponding

equivalent viscous damping ratios ζ per Eq. (4) with a number of impacts n of 2. Accordingly, this estimation of equivalent viscous damping ratio ζ captured the total energy loss over a full cycle of motion and showed how this loss varied with respect to the lateral drift amplitudes. Experimental results of equivalent viscous damping ratio ζ are presented in Fig. 5 as a function of several measured drift amplitudes. In all cases, the data showed that the equivalent viscous damping ratio ζ increases for lower drift amplitudes. This behavior has also been observed in previous tests of precast concrete members²⁷ and can be attributed to the increase in the member-to-foundation contact with decreasing lateral drift.

It is also seen in Fig. 5 that equivalent viscous damping ratio ζ in the test system with grout was below 3% for drift amplitudes higher than 0.6%, while the equivalent viscous damping ratio ζ in the test systems with rubber was higher and, in several cases, increased by an order of magnitude from the equivalent viscous damping ratio ζ in the test system with grout. For practical purposes, there was no significant effect of the shore hardness SH on equivalent viscous damping ratio ζ , while equivalent viscous damping ratio ζ increased with the rubber thickness, with the increase being more significant between the layer thicknesses of 25.4 and 12.7 mm (1 and 0.5 in.). Table 2 presents the average equivalent viscous damping ratio ζ values, which were computed using the data in Fig. 5 with respect to three ranges of lateral drift amplitude: 0% to 1%, 1% to 2%, and 2% to 3%. All values are shown to increase with decreasing drift amplitude. It is also seen that equivalent viscous damping ratio ζ did not vary significantly with respect to the shore hardness SH of the rubber. When the rubber with a shore hardness SH of 50 was used, the equivalent viscous damping ratio ζ increased with the rubber thickness. Overall, the use of rubber layers increased the equivalent viscous damping ratio in the test systems by more than a factor of 2.

Components of energy loss Per Housner,¹¹ rocking members with rigid jointed connections exhibit no energy loss due

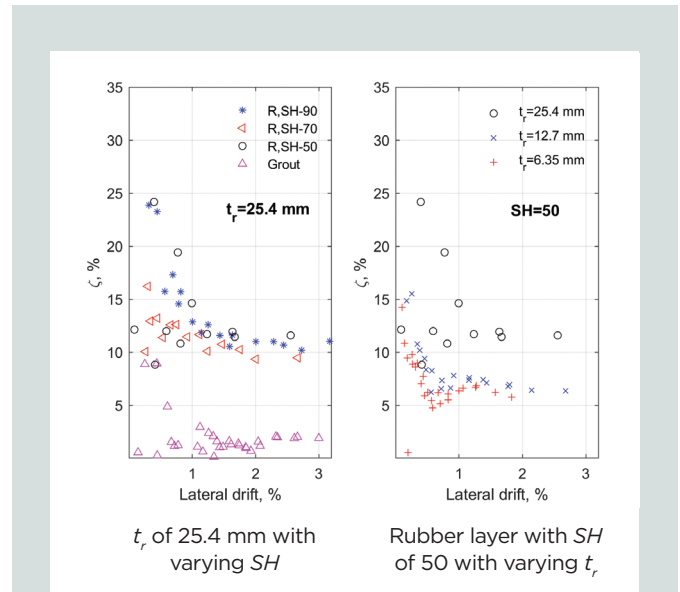


Figure 5. Equivalent viscous damping ratio ζ of test systems with rubber thickness t_r of 25.4 mm with varying shore hardness SH and rubber layer with a shore hardness SH of 50 with varying rubber thickness t_r . Note: R = rubber. 1 mm = 0.0394 in.

to flexure, hysteresis, or friction at the connections, but all losses occur during the impacts. Kalliontzis and Sritharan¹⁰ found this assumption to be reasonable for free vibration tests of precast concrete members with unbonded post-tensioning that use grout at the jointed connection. This section investigates how this behavior can be altered by placing rubber layers at the jointed connections. For this purpose, the energy components associated with the rocking responses of the precast concrete member were computed. These included rotational kinetic energy K , gravitational potential energy U^g , and strain energy in the unbonded post-tensioning tendon U_{PT}^s .

$$K = \frac{1}{2} I_o \dot{\theta}^2 \quad (6)$$

Table 2. Experimentally measured average values of equivalent damping ratio ζ for three ranges of lateral drift amplitude

Material	Shore hardness SH	Thickness, mm	Measured average values of ζ per drift amplitude, %		
			2% to 3%	1% to 2%	0% to 1%
Grout	n/a	25.4	1.8	1.4	3.5
Rubber	50	6.35	n.d.	6.5	7.3
Rubber	50	12.7	6.4	7.2	9.3
Rubber	50	25.4	11.6	11.7	19.8
Rubber	70	25.4	9.4	10.7	12.6
Rubber	90	25.4	10.4	11.9	18.4

Note: n/a = not applicable; n.d. = no data. 1 mm = 0.0394 in.

$$U_g = MgR_0 [\cos(a - |\theta|) - \cos a] \quad (7)$$

$$U_{PT} = \frac{L}{2AE} F_{PT}^2 \quad (8)$$

where

$\dot{\theta}$ = angular velocity of the precast concrete member

L = unbonded length of the tendon

A = cross-sectional area of the unbonded tendon

E = modulus of elasticity of the unbonded tendon

= 198,600 MPa (28,800 ksi)

F_{PT} = total force exerted by the unbonded tendon

Using Eq. (6) through (8), the total energy content in the precast concrete member E_{total} was computed using Eq. (9):

$$E_{total} = K + U_g + U_{PT} \quad (9)$$

Time histories of the total energy content in the precast concrete member E_{total} in the test systems with rubber are presented in Fig. 6. For a better comparison between the different systems, the presented responses of the total energy content in the precast concrete member E_{total} excluded the constant energy introduced by the initial post-tensioning forces because these forces differed from one system to another, as shown in Table 1. In addition to the experimental total energy content in the precast concrete member E_{total} , Fig. 6 includes the theoretical responses of a controlled rocking model (CRM),¹⁰ which has been experimentally verified for accurately computing the responses of precast concrete members with a grout layer at the jointed connection. Based on the theoretical responses, total energy content in the precast concrete member E_{total} reduces instantaneously at every impact due to the impact energy loss but remains constant during the rest of the rocking motion. A different behavior, however, is seen in the experimental total energy content in the precast concrete member E_{total} during both the impact and the nonimpact phases of the rocking motion.

During the impacts, the experimental total energy content in the precast concrete member E_{total} drops completely and recovers partially, causing energy loss at each impact. The significant drop in total energy content in the precast concrete member E_{total} during the impacts could be artificial and stem from noise in the data acquisition system, as also observed in previous tests by Kalliontzis and Sritharan.²⁷ During the nonimpact phases of motion, the experimental total energy content in the precast concrete member E_{total} does not stay constant as in the CRM.¹⁰ This is attributed to the rubber layers at the jointed connections, which are not considered in the CRM.¹⁰ Due to the presence of the rubber layers, strain energy is stored within the rubber, which is not accounted for in the calculation of total energy content in the precast concrete

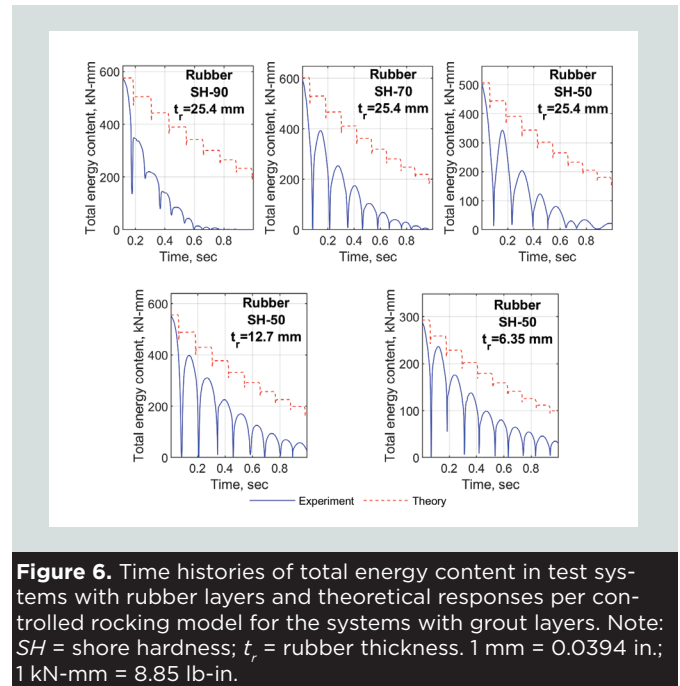


Figure 6. Time histories of total energy content in test systems with rubber layers and theoretical responses per controlled rocking model for the systems with grout layers. Note: SH = shore hardness; t_r = rubber thickness. 1 mm = 0.0394 in.; 1 kN-mm = 8.85 lb-in.

member E_{total} per Eq. (9). During the rocking motion, there is a continuous energy transfer between the total energy content in the precast concrete member E_{total} stored in the precast concrete member and the strain energy stored in the rubber, ultimately producing energy loss for the precast concrete member over a full cycle of motion. The energy transferred between the precast concrete member and the rubber becomes more evident with decreasing shore hardness and increasing thickness of the rubber, and it agrees with previous free vibration tests of a freestanding rocking member (that is, without unbonded post-tensioning) with rubber layers at the jointed connection.²⁸

Therefore, it can be stated that compared with the CRM,¹⁰ the use of rubber layers introduces different energy-dissipation components, which are associated with the impact and the nonimpact phases of rocking motion. To estimate the energy loss during the impact phases, the time histories of kinetic energy in the test systems were computed using Eq. (6). Using these time histories, the energy loss during the impacts ΔE_{impact} was calculated as follows:⁹

$$\Delta E_{impact} = (1 - r_{exp}) K_{impact}$$

where

r_{exp} = experimentally estimated coefficient of restitution per impact event

K_{impact} = kinetic energy of the test system just before the impact, computed with Eq. (6)

Table 3 presents the percentages of impact energy loss over the total energy loss at the end of the rocking motions. The table shows that impact energy loss in the test systems was a small portion of the total energy loss, indicating that continuous ener-

gy loss within the rubber layers dominated the decay of energy. It is observed that impact energy loss increased with the shore hardness SH and reduced with the rubber thickness, but in all cases, it contributed less than 30% of the total energy loss.

Overall, these comparisons show that thin rubber layers improve the damping capability of precast concrete members. Nevertheless, it is shown in the next sections that thin rubber layers with higher shore hardness SH are more desirable because they provide the necessary damping without compromising the lateral stiffness, strength, and overall seismic behavior of the precast concrete members.

Post-tensioning forces This section investigates the increase of the post-tensioning forces in the test systems as a function of the different rubber layers and the grout layer, as shown in Fig. 7. The post-tensioning force in the test system with rubber with a shore hardness SH of 90 was occasionally higher than the post-tensioning force in the system with grout. This difference is partly attributed to the energy transfer taking place between the precast concrete member and the rubber layer, as explained earlier in this paper. This energy transfer could have caused vertical oscillations in the precast concrete member, increasing the post-tensioning force during the uplifting phase of the rocking motions.

Comparisons between the test systems with rubber show that decreasing the shore hardness SH or increasing the thickness of the layer reduced the post-tensioning forces developed in the systems. These lower post-tensioning forces were, in part, attributed to the larger neutral axis depth NAD at the jointed connection, which produced lower elongations in the tendon. For example, at a lateral drift of 2%, the neutral axis depth NAD values in the test systems with rubber with a shore hardness SH of 50 and thicknesses of 25.4, 12.7, and 6.35 mm (1, 0.5, and 0.25 in.) were measured to be 53, 42.7, and 36 mm (2.1, 1.7, 1.42 in.), respectively, as calculated from the bottom corner of the member. At the same lateral drift, the neutral axis depth NAD values in the test systems with rubber with a shore hardness SH of 70 and 90 and thickness of 25.4 mm were measured to be 35.6 mm (1.4 in.) and 12.7 mm, respectively, while a neutral axis depth NAD value of 17.8 mm (0.7 in.) was measured in the test system with the grout interface. A larger value of neutral axis depth NAD was measured for the grout interface than the rubber with a shore hardness SH of 90, which should be expected based on the preceding discussion, emphasizing the existence of vertical oscillations in the precast concrete member. However, for practical purposes, the use of rubber with a shore hardness SH of 90 did not alter the post-tensioning force and neutral axis depth NAD behaviors with respect to the grout interface.

Force-displacement responses Using the previously referenced experimental measurements of neutral axis depth NAD and in the absence of experimental data of lateral forces, the authors made an attempt to analytically reproduce the force-displacement responses of the test systems up to a lateral drift of 3%. The following assumptions were used:

Table 3. Contribution of impact energy loss over the total energy loss in the test systems with rubber layers

Material	Shore hardness SH	Thickness, mm	Impact energy loss, %
Rubber	50	6.35	29.4
Rubber	50	12.7	26.0
Rubber	50	25.4	18.9
Rubber	70	25.4	23.0
Rubber	90	25.4	29.7

Note: 1 mm = 0.0394 in.

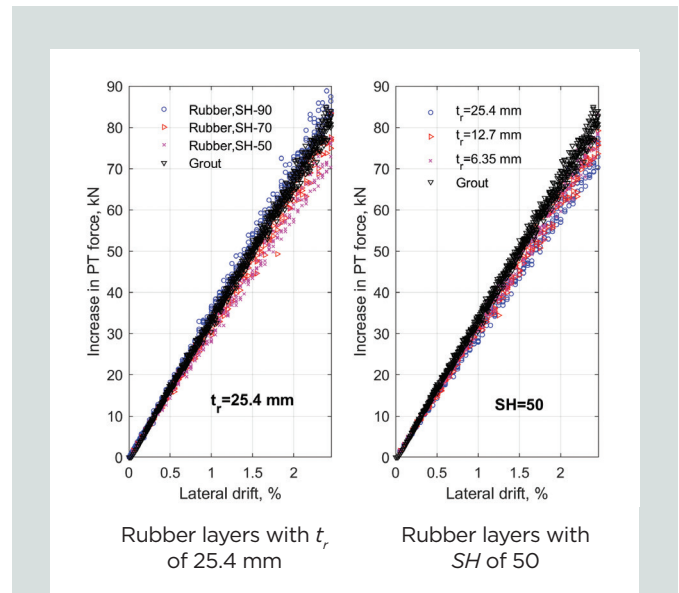


Figure 7. Increase in post-tensioning force as a function of the lateral drifts undergone by the test systems with grout and rubber thickness t_r of 25.4 mm with varying shore hardness SH and rubber layers with a shore hardness SH of 50 with varying rubber thickness t_r . Note: 1 mm = 0.0394 in.; 1 kN = 0.225 kip.

- Considering that no inelastic action was recorded within the precast concrete members, material layers, or foundation, the compressive stress at the jointed connection was assumed to follow a linear distribution along the neutral axis depth NAD , which produced a resultant compressive force at a distance of $NAD/3$ from the bottom corner of the members.
- Based on the data in Fig. 7, the unbonded tendons did not exceed the proportional stress limit.

Accordingly, the lateral force applied at the top of the test systems $F(\theta)$ was estimated as follows:

$$F(\theta) = \frac{Mg\bar{R}\sin(\bar{\alpha} - |\theta|) + \left(F_{PTi} + \frac{AE}{L} \delta L \right) \left(\frac{b}{2} - \frac{NAD}{3} \right)}{h}$$

where

\bar{R} = distance of resultant compressive force at the member base from center of gravity of the precast concrete member

\bar{a} = slenderness coefficient with respect to the location of the resultant compressive force at the member base

F_{PTi} = initial post-tensioning force

δL = elongation of the unbonded tendon due to the angular displacement of the precast concrete member = $(b - NAD)|\theta|$

$$\bar{a} = \tan^{-1} \left(\frac{\frac{b - NAD}{2} - \frac{3}{h}}{\frac{h}{2}} \right)$$

$$\bar{R} = \sqrt{\left(\frac{h}{2}\right)^2 + \left(\frac{b - NAD}{3}\right)^2}$$

The neutral axis depth NAD is computed as a function of the rotation θ using the analytical approach detailed by Kalliontzis and Sritharan.¹⁰ In this approach, the lateral response varies with the length of the neutral axis depth NAD , which is different for the cases of rubber and grout interfaces. To compare the force resistance provided by the different test systems, an initial post-tensioning force of 17.8 kN (4 kip) was assumed in the analyses of all test systems.

Figure 8 presents the analytically estimated force-displacement responses. Due to the small differences in the variation of post-tensioning forces, the system with rubber with a shore hardness SH of 90 was comparable to the use of grout only at the jointed connection. However, a decrease in the shore hardness SH below 90 or an increase in the rubber thickness reduced the lateral-force resistance of the test system. Accordingly, the lowest lateral force occurred when the rubber with a shore hardness SH of 50 and layer thickness of 25.4 mm (1 in.) was used. This system exhibited a reduction by 12.1% at a lateral drift of 2% when compared with the system with grout.

Analytical investigation

This section investigates the seismic responses of the test systems with rubber using a simplified SDOF model. This model is based on Eq. (1), which is modified to account for the continuous energy loss induced by the rubber, the recentering force by unbonded post-tensioning, and impact energy loss per Eq. (3). This section includes comparisons with precast concrete members that use grout layers at the jointed connections.

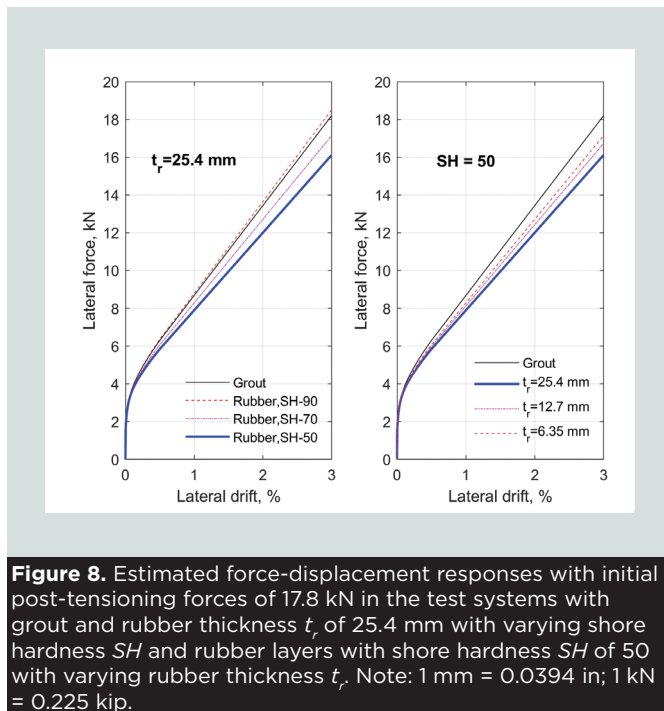


Figure 8. Estimated force-displacement responses with initial post-tensioning forces of 17.8 kN in the test systems with grout and rubber thickness t_r of 25.4 mm with varying shore hardness SH and rubber layers with shore hardness SH of 50 with varying rubber thickness t_r . Note: 1 mm = 0.0394 in; 1 kN = 0.225 kip.

Single-degree-of-freedom model

The SDOF model assumes that there is energy transfer between the precast concrete member and the rubber layers during the nonimpact phases of motion, which agrees with the experimental observations discussed in this paper. This energy transfer ultimately causes some continuous energy loss in the member, in addition to the impact energy loss. The equation of motion of the SDOF model is as follows:

$$I_0 \ddot{\theta} + MgR_0 \sin[\text{sign}(\theta)a - \theta] + M_{PT} + M_c = -MR\ddot{u}_g \cos[\text{sign}(\theta)a - \theta]$$

where

M_{PT} = recentering moment induced by the unbonded post-tensioning tendon

M_c = moment induced by the continuous energy transfer mechanism, which is assumed to be a function of the square root of the angular velocity. This function was empirically selected because it provides a close correlation of the SDOF model to the experimental results, as shown later in this paper.

$$M_c = B[\text{sign}(\theta), \text{sign}(\dot{\theta})] \sqrt{|\dot{\theta}|}$$

$$M_{PT} = \text{sign}(\theta) \left[\left(F_{PTi} + \frac{AE}{L} \lambda b \tan |\theta| \right) \right] (\lambda b)$$

where

B = modeling parameter defining the magnitude of M_c

$\text{sign}(\dot{\theta})$ = sign of angular velocity

Table 4. Estimated parameters for the single-degree-of-freedom model of the test systems with rubber layers

Shore hardness SH	Thickness, mm	λ	$B[+, -]/I_o$	$B[+, +]/I_o$	$B[-, -]/I_o$	$B[-, +]/I_o$
50	6.35	0.90	-6.6	-5.3	5.3	6.6
50	12.7	0.88	-8.6	-6.9	6.9	8.6
50	25.4	0.85	-12.5	-10.0	10.0	12.5
70	25.4	0.90	-11.6	-8.9	8.9	11.6
90	25.4	1.00	-7.8	-2.0	2.0	7.8

Note: B = modeling parameter defining the magnitude of M_c in units of $\text{kN}\cdot\text{mm}\sqrt{\text{sec}}$; I_o = mass moment of inertia of the rocking member about its pivot point; M_c = moment induced by the continuous energy transfer mechanism; λ = modeling parameter defining the magnitude of the tendon elongation due to the angular displacement of the precast concrete member. 1 mm = 0.0394 in.; 1 kN = 0.225 kip.

λ = modeling parameter defining the magnitude of the tendon elongation due to the angular displacement of the precast concrete member

Table 4 presents the values of the empirical parameters λ and B as calibrated with the experimental data. As shown in this table, a different value for the modeling parameter defining the magnitude of the moment induced by the continuous energy transfer mechanism B was assigned per rocking phase, where a rocking phase is defined in terms of the sign of angular displacement $\text{sign}(\theta)$ and sign of angular velocity $\text{sign}(\dot{\theta})$. The selected values of the modeling parameter defining the magnitude of the moment induced by the continuous energy transfer mechanism B are presented in Table 4 as normalized with respect to the mass moment of inertia of the rocking member about its pivot point I_o of the precast concrete member. The selected values of the modeling parameter defining the magnitude of the moment induced by the continuous energy transfer mechanism B are symmetric with respect to the positive and negative directions of rocking motion.

The selected variation in the modeling parameter defining the magnitude of the moment induced by the continuous energy transfer mechanism B was established based on experimental evidence of the test systems with rubber and is explained in **Fig. 9** and **10**. Figure 9 presents experimental responses of a phase diagram, which is the relationship between the angular displacements and velocities of the precast concrete member; Fig. 10 presents the time history of E_{total} . In each case, four phases of a rocking motion are included, completing a full cycle.

According to Fig. 9 and 10, a precast concrete member with a rubber layer at the jointed connection loses energy into this layer during the first phase of rocking motion. Next, during the second phase, it impacts with the base, uplifts, and regains part of the strain energy stored within the rubber layer in the form of kinetic energy until it reaches its peak angular displacement and zero angular velocity. During the third phase, the member undergoes energy loss and it subsequently impacts with the base. It then enters the fourth phase, during which it undergoes energy gain. It is emphasized that the observed energy gain during the second and fourth phases represents the net energy

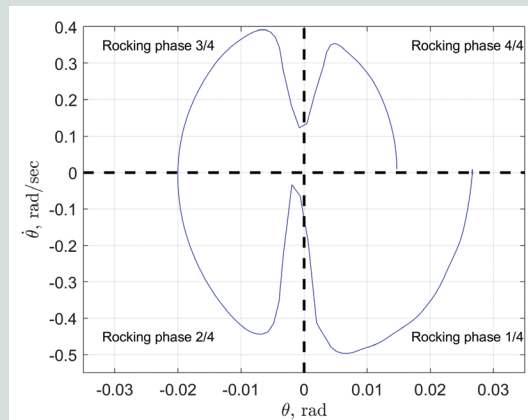


Figure 9. Phase diagram during a full rocking cycle of the system with rubber layer with a shore hardness SH of 70. Note: B = modeling parameter defining the magnitude of M_c in units of $\text{kN}\cdot\text{mm}\sqrt{\text{sec}}$; I_o = mass moment of inertia of the rocking member about its pivot point; M_c = moment induced by the continuous energy transfer mechanism; θ = angular displacement of the precast member; $\dot{\theta}$ = angular velocity of the precast concrete member.

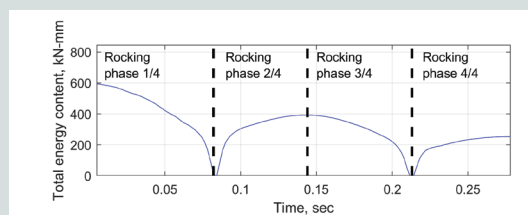


Figure 10. Total energy content during a full rocking cycle of the system with rubber layer with a shore hardness SH of 70. Note: 1 kN-mm = 8.85 lb-in.

transfer between the precast concrete member and the rubber layer; it is expected that part of the kinetic energy transferred into the rubber is also dissipated during these two phases.

Verification The developed SDOF model was used to reproduce the free vibration responses of all test systems with

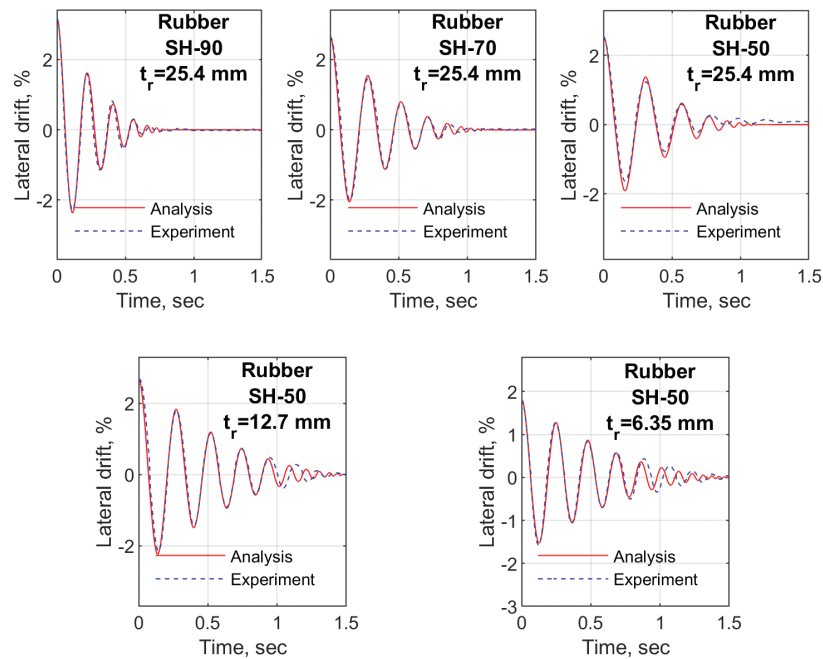


Figure 11. Comparisons between experimental lateral drift responses and the single-degree-of-freedom model. Note: *SH* = shore hardness; t_r = rubber thickness. 1 mm = 0.0394 in.

rubber using the same initial conditions as in the experimental investigation. Comparisons between experimentally measured and analytical time histories of lateral drift are presented in **Fig. 11**. The figure shows that the SDOF model agreed well with the experimental responses for all test systems. The model captured the responses satisfactorily over several cycles, and some deviations occurred only at small lateral drift amplitudes, below 0.25%.

Base motion This section uses the SDOF model to investigate the responses of precast concrete members with rubber layers to horizontal ground excitations. Considering that increasing the rubber thickness and decreasing its shore hardness *SH* reduce the lateral stiffness and strength of the precast concrete members, as shown in Fig. 8, the following investigation examines the following two rubber layers:

- thickness of 25.4 mm (1 in.) and shore hardness *SH* of 90
- thickness of 6.35 mm (0.25 in.) and shore hardness *SH* of 50

The responses of these members are also compared with the controlled-rocking model of CRM-II,²⁹ which modifies the CRM¹⁰ to account for controlled-rocking motions at large lateral drifts of precast concrete members with grout interfaces. Details of the CRM-II can be found in Kalliontzis.²⁹

The SDOF models and CRM-II for controlled-rocking motions with rubber and grout interfaces, respectively, were excited using two scaled earthquake records from Nazari

et al.,^{30,31} which represented the Chile earthquake in 2010 as recorded by the Santiago Station and the Kobe, Japan, earthquake in 1995 as recorded by the Takatori Station. Time histories of the corresponding horizontal ground excitations can be found in Nazari et al.^{30,31}

The corresponding responses by the CRM-II and the previously referenced SDOF model representing the test systems with grout and rubber layers, respectively, are presented in **Fig. 12** and **13**. An initial post-tensioning force of 17.8 kN (4 kip) was assumed in all test systems. As shown in Fig. 12, the largest (absolute) peak lateral drift of 2.04% for Chile was reached by the CRM-II, followed by a peak drift of 1.7% in the test system with rubber with a shore hardness *SH* of 50. The lowest peak drift of 1.4% was attributed to the test system with rubber with a shore hardness *SH* of 90. In all cases, the test systems with rubber reduced the responses of the precast concrete member due to this excitation. Similar differences between the test systems can be noted for Kobe, Japan, in Fig. 13.

Further insight into the seismic behavior of precast concrete members with rubber layers can be obtained using the uplift spectra.³² These spectra compute the peak seismic drifts of precast concrete members with different slenderness, size, and initial post-tensioning force. Uplift spectra for the same two ground motions were computed using the following parameters:

- A concentric unbonded post-tensioning tendon with diameter of 15.24 mm (0.6 in.) was used, as in the experimental investigation.

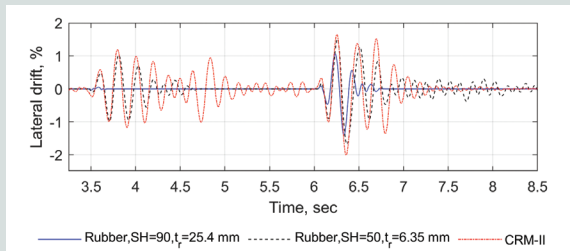


Figure 12. Analytically estimated responses to the Chile earthquake of 2010 recorded by the Santiago Station. Note: CRM-II = controlled-rocking model for large lateral drifts of precast concrete members; SH = shore hardness; t_r = rubber thickness. 1 mm = 0.0394 in.

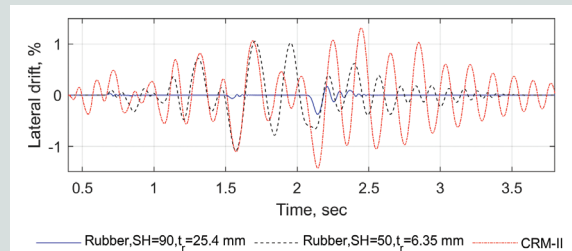


Figure 13. Analytically estimated responses to the Kobe, Japan, earthquake of 1995 recorded by the Takatori Station. Note: CRM-II = controlled-rocking model for large lateral drifts of precast concrete members; SH = shore hardness; t_r = rubber thickness. 1 mm = 0.0394 in.

- The initial post-tensioning force-to-weight ratio F_{PT}/Mg was selected to remain constant throughout an uplift spectrum, which is consistent with previous research.³² A post-tensioning force-to-weight ratio F_{PT}/Mg of 1.9 was used, which is the same as in the analyses of Fig. 14 and 15.
- Two slenderness ratios were used for the precast concrete members:
 - The slenderness ratio h/b of 3.41 is the same as that of the precast concrete member in the experimental investigation.
 - A higher slenderness ratio h/b of 6.00 was also used. The value of the slenderness ratio h/b remained constant throughout an uplift spectrum.

Figures 14 and 15 present the uplift spectra for the two excitations and the range $1 < 2\pi/p < 5$ seconds (where p is the dynamic parameter of the rocking member), an increase in the parameter $2\pi/p$ corresponds to an increase in the size of the precast concrete member.³² Overall, the use of rubber with a shore hardness SH of 90 reduced the peak drifts compared with CRM-II. For example, during the Chile earthquake and a height-to-width ratio h/b of 6.00, the system with rubber with a shore hardness SH of 90 underwent its maximum peak drift of 2.6% at $2\pi/p$ of 2.0 seconds, while at a $2\pi/p$, the CRM-II experienced a peak drift of 7.4%. For the Kobe, Japan, earthquake and a height-to-width ratio h/b of 6.00, the system with rubber with a shore hardness SH of 90 underwent its maximum peak drift of 2.8% at a $2\pi/p$ of 2.8 seconds, while the CRM-II underwent a peak drift of 6.9% for the same value of $2\pi/p$. For the present range of responses, the use of rubber with a shore hardness SH of 90 reduced the seismic responses below 3.0% drifts throughout the spectra. Instead, the CRM-II underwent drifts as high as 9.0% (that is, Kobe, Japan, earthquake and a height-to-width ratio h/b of 6.00). On the other hand, the system with a shore hardness SH of 50 exhibited a different behavior. This system did not produce consistent responses with respect to the CRM-II. In many cases, its peak drifts were comparable to those of the CRM-II or higher. More important, the uplift spectra estimated that this system may overturn, which occurred when the

lines of the spectra exceeded the upper limits of peak drift in the figures. This behavior translates into the collapse of the structural system and is attributed to the continuous energy transfer occurring during uplifting of the precast concrete member, which was explained in Fig. 9 and 10. As also discussed in Fig. 6, this energy transfer had a larger effect in the case of a rubber interface with a shore hardness SH of 50 than with a shore hardness SH of 90, which can amplify the associated seismic responses, as observed in Fig. 14 and 15.

Conclusion

The present research study investigated the use of rubber layers to mitigate the seismic response of precast concrete members with jointed connections. Experiments showed that the use of rubber layers with thicknesses of 6.35 to 25.4 mm (0.25 to 1 in.) and a shore hardness SH of 50 to 90 can improve the damping capability of precast concrete members; however, it was also found that a reduced shore hardness SH (<90) may not be desirable because it could compromise the members' lateral stiffness, force resistance, and seismic behavior.

When a rubber layer with a shore hardness SH of 90 and thickness of 25.4 mm (1 in.) was tested, the resulting system exhibited comparable force-displacement behavior to that obtained using grout at the jointed connection. This system provided average damping ratios from 10.4% to 18.4% in the range of lateral drifts up to 3%. This was a significant improvement over the system with grout at the jointed connection, which provided average damping ratios from 1.8% to 3.5%.

To estimate the effect of rubber layers in the seismic response of precast concrete members, an SDOF model was developed. The model was verified using the experimental data of this research study and was employed to investigate the seismic response of precast concrete members with the following attributes:

- a shore hardness SH of 90 and a thickness of 25.4 mm (1.0 in.)
- a shore hardness SH of 50 and a thickness of 6.35 mm (0.25 in.)

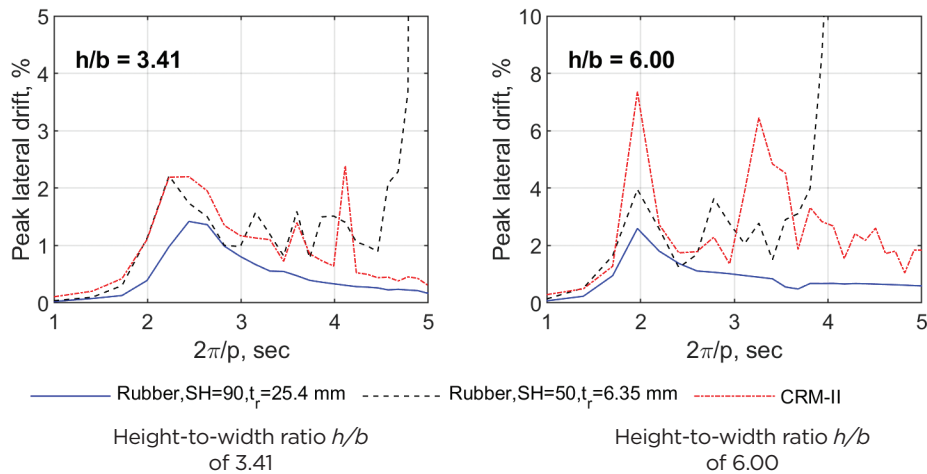


Figure 14. Uplift spectra for Chile earthquake of 2010 recorded by the Santiago Station. Note: b = base width of precast concrete member; CRM-II = controlled-rocking model for large lateral drifts of precast concrete members; h = height of precast concrete member; ρ = dynamic parameter of the rocking member; SH = shore hardness; t_r = rubber thickness. 1 mm = 0.0394 in.

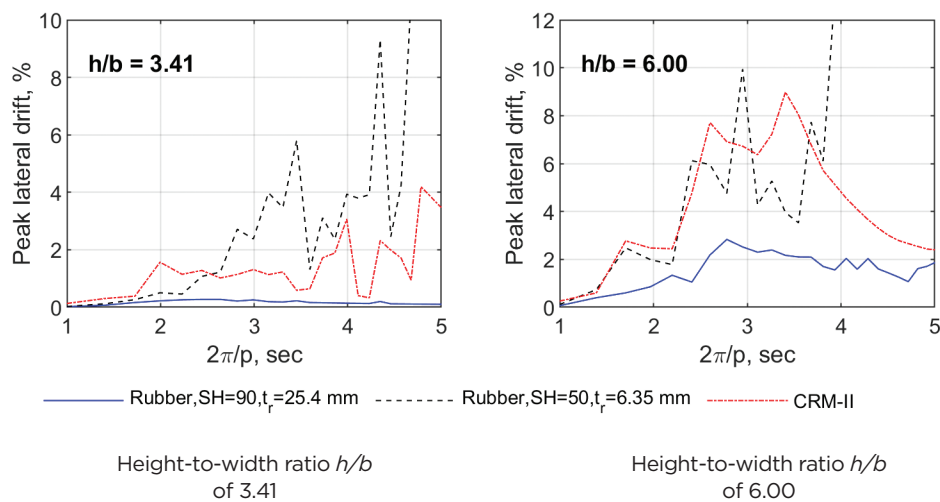


Figure 15. Uplift spectra for Kobe, Japan, earthquake of 1995 recorded by the Takatori Station. Note: b = base width of precast concrete member; CRM-II = controlled-rocking model for large lateral drifts of precast concrete members; h = height of precast concrete member; ρ = dynamic parameter of the rocking member; SH = shore hardness; t_r = rubber thickness. 1 mm = 0.0394 in.

Included were comparisons with the use of grout at the jointed connection. Two horizontal ground excitations were used for this purpose, providing accelerations as high as $1.42g$, where g is acceleration due to gravity. Analytical results of uplift spectra showed that the use of rubber with a shore hardness SH of 90 reduced the seismic responses throughout the spectra compared with the use of grout. In all responses and for the selected ground excitations, all peak lateral drifts of the precast concrete members that used this rubber class were below 3%. Different responses were produced with the use of rubber with a shore hardness SH of 50, which, in

many cases resulted in the collapse of the precast concrete members.

Based on the range of experimental data and analytical simulations examined in this paper, rubber layers with a shore hardness SH of 90 or greater and thickness in the range of 6.35 to 25.4 mm (0.25 to 1 in.) are recommended to improve the damping capability in precast concrete members. Further research would help identify suitable properties of rubber for cases that could be established with precast concrete members of different geometric properties subjected to shake-table testing.

Acknowledgments

The work presented in this paper was undertaken as part of the Network for Earthquake Engineering Simulations Rocking Wall Project with funding from the National Science Foundation (NSF) under grant 1041650 and a 2013 Daniel P. Jenny fellowship from PCI. Joy Pauschke served as the program manager for the NSF grant. Any opinions, findings, and conclusions or recommendations expressed in this material are those of the authors and do not necessarily reflect the views of the NSF or PCI.

References

- Schultz, A. E., G. S. Cheok, and R. A. Magana. "Performance of Precast Concrete Shear Walls." Paper presented at the Sixth U.S. National Conference on Earthquake Engineering in Seattle Wash., May and June 1998.
- Priestley, M. J. N., S. Sritharan, J. R. Conley, and S. Pampanin. 1999. "Preliminary Results and Conclusions from the PRESSS Five-Story Precast Concrete Test Building." *PCI Journal* 44 (6): 42–67.
- Nakaki, S. D., J. F. Stanton, and S. Sritharan. 1999. "An Overview of the PRESSS Five-Story Precast Test Building." *PCI Journal* 44 (2): 26–39.
- Kurama, Y., R. Sause, S. Pessiki, and L. W. Lu. 1999. "Lateral Load Behavior and Seismic Design of Unbonded Post-tensioned Precast Concrete Walls." *ACI Structural Journal* 96 (4): 622–632.
- Perez, F., S. Pessiki, and R. Sause. 2004. "Experimental and Analytical Lateral Load Response of Unbonded Post-tensioned Precast Concrete Walls." ATLSS report 04-11. Bethlehem, PA: Lehigh University.
- Sritharan, S., S. Aaleti, R. H. Henry, K. Y. Liu, and K. C. Tsai. 2015. "Precast Concrete Wall with End Columns (PreWEC) for Earthquake Resistant Design." *Earthquake Engineering and Structural Dynamics* 44 (12): 2075–2092.
- Twigden, K., S. Sritharan, and R. S. Henry. 2017. "Cyclic Testing of Unbonded Post-tensioned Concrete Wall Systems with and without Supplemental Damping." *Engineering Structures* 140: 406–420.
- Nazari, M., S. Sritharan, and S. Aaleti. 2016. "Single Precast Concrete Rocking Walls as Earthquake Force-Resisting Elements." *Earthquake Engineering and Structural Dynamics* 46 (5): 753–769.
- Kalliontzis, D., S. Sritharan, and A. E. Schultz. 2016. "Improved Coefficient of Restitution Estimation for Free Rocking Members." *Journal of Structural Engineering* 142 (12). [https://doi.org/10.1061/\(ASCE\)ST.1943-541X.0001598](https://doi.org/10.1061/(ASCE)ST.1943-541X.0001598).
- Kalliontzis, D., and S. Sritharan. 2020. "Dynamic Response and Impact Energy Loss in Controlled Rocking Members." *Earthquake Engineering and Structural Dynamics* 49 (6): 319–338.
- Housner, G. W. 1963. "The Behavior of Inverted Pendulum Structures during Earthquakes." *Bulletin of the Seismological Society of America* 53 (2): 403–417.
- Priestley, M. J. N., R. J. Evison, and A. J. Carr. 1978. "Seismic Response of Structures Free to Rock on Their Foundations." *Bulletin of the New Zealand National Society for Earthquake Engineering* 11 (3): 141–150.
- Muto, K., H. Umemura, and Y. Sonobe. 1960. "Study of the Overturning Vibration of Slender Structures." *Proceedings of the 2nd World Congress on Earthquake Engineering*. Tokyo, Japan. 1239–1261.
- Ogawa, N. 1977. *A Study on Rocking and Overturning of Rectangular Column*. Report 18. Tokyo, Japan: National Research Center for Disaster Prevention.
- Aslam, M., W. G. Godden, and D. T. Scalise. 1980. "Earthquake Rocking Response of Rigid Bodies." *Journal of the Structural Division* 106: 377–392.
- Lipscombe, P. R., and S. Pellegrino. 1993. "Free Rocking of Prismatic Blocks." *Journal of Engineering Mechanics* 119: 1387–1410.
- Fielder, W. T., L. N. Virgin, and R. H. Plaut. 1997. "Experimental and Simulation of Overturning of an Asymmetric Rocking Block on an Oscillating Foundation." *European Journal of Mechanics and Solids* 16: 905–923.
- Peña, F., F. Prieto, P. B. Lourenco, A. C. Costa, and J. V. Lemos. 2007. "On the Dynamics of Rocking Motion of Single Rigid-Block Structures." *Earthquake Engineering and Structural Dynamics* 36 (15): 2383–2399.
- Ma, Q. T. M. 2009. "The Mechanics of Rocking Structures Subjected to Ground Motion." PhD thesis, Department of Civil and Environmental Engineering, University of Auckland, New Zealand.
- O'Hagan, J., K. Twigden, and Q. T. M. Ma. 2013. "Sensitivity of Post-tensioned Concrete Wall Response to Modeling of Damping." In *Proceedings, New Zealand Society for Earthquake Engineering Conference*. Wellington, New Zealand: New Zealand Society for Earthquake Engineering.
- Kalliontzis, D. 2014. "Dynamic Decay of Motion of Rocking Concrete Members." MSc thesis, Iowa State University.

22. Chopra, A. K. *Dynamics of Structures: Theory and Applications to Earthquake Engineering*. 5th ed. Des Moines, IA: Pearson.
23. Makris, N., and D. Konstantinidis. 2002. "The Rocking Spectrum and the Limitation of Design Guidelines." *Proceedings of the 15th ASCE Engineering Mechanics Conference*.
24. Twigden, K. M. 2016. "Dynamic Response of Unbonded Post-tensioned Concrete Walls for Seismic Resilient Structures." PhD thesis, Department of Civil and Environmental Engineering, University of Auckland, New Zealand.
25. Cheng, C. T. 2007. "Energy Dissipation in Rocking Bridge Piers under Free Vibration Tests." *Earthquake Engineering and Structural Dynamics* 36 (4): 503–518.
26. ACI (American Concrete Institute) Innovation Task Group 5. 2008. *Acceptance Criteria for Special Unbonded Post-tensioned Precast Structural Walls Based on Validation Testing and Commentary*. ACI ITG-5.1-07. Farmington Hills, MI: ACI.
27. Kalliontzis, D., and S. Sritharan. 2018. "Characterizing Dynamic Decay of Motion of Free-Standing Rocking Members." *Earthquake Spectra* 34 (2): 843–866.
28. Elgawady, M. A., Q. Ma, J. W. Butterworth, and J. Ingham. 2011. "Effects of Interfaces Material on the Performance of Free Rocking Blocks." *Earthquake Engineering and Structural Dynamics* 40: 375–392.
29. Kalliontzis, D. 2018. "Behavior of Precast Concrete and Masonry Wall Systems with Jointed Connections Subjected to Lateral Loads." PhD diss., Department of Civil, Environmental, and Geo- Engineering, University of Minnesota.
30. Nazari, M., S. Aaleti, and S. Sritharan. 2015. "Shake Table Testing of Precast Rocking Wall with End column_1 (PreWEC1) @ UNR." Experimental data. Network for Earthquake Engineering Simulation. <https://doi.org/10.17603/DS2RW24>.
31. Nazari, M., S. Aaleti, and S. Sritharan. 2015. "Shake Table Testing of Single Rocking Wall_1 (SRW1) @ UNR." Experimental data. Network for Earthquake Engineering Simulation. <https://doi.org/10.4231/D3N29P75Z>.
32. Vassiliou, M. F., and N. Makris. 2015. "Dynamics of the Vertically Restrained Rocking Column." *Journal of Engineering Mechanics* 141 (12). [https://doi.org/10.1061/\(ASCE\)EM.1943-7889.0000953](https://doi.org/10.1061/(ASCE)EM.1943-7889.0000953).

Notation

a	= slenderness coefficient of the rocking member
\bar{a}	= slenderness coefficient with respect to the location of the resultant compressive force at the member base
A	= cross-sectional area of the unbonded tendon
b	= base width of precast concrete member
B	= modeling parameter defining the magnitude of M_c
E	= modulus of elasticity of the unbonded tendon
E_{total}	= total energy content in the precast concrete member
F_{PT}	= total force exerted by the unbonded tendon
F_{PTi}	= initial post-tensioning force
$F(\theta)$	= lateral force applied at the top of the test systems
g	= acceleration due to gravity
h	= height of precast concrete member
I_o	= mass moment of inertia of the rocking member about its pivot point
k	= ratio of the distance between the pivot points just before and just after impact over the member's base width
K	= rotational kinetic energy of the precast concrete member
K_{impact}	= kinetic energy of the test system just before the impact
K_1	= kinetic energy of the rocking member just before the impact event
K_2	= kinetic energy of the rocking member just after the impact event
L	= unbonded length of the tendon
M	= total mass of the rocking member
M_c	= moment induced by the continuous energy transfer mechanism
M_{PT}	= recentering moment induced by the unbonded post-tensioning tendon
n	= number of impacts

- NAD = neutral axis depth at the jointed connection
- p = dynamic parameter of the rocking member
- r = coefficient of restitution
- r_{exp} = experimentally estimated coefficient of restitution per impact
- R = rubber
- \bar{R} = distance of resultant compressive force at the member base from center of gravity of the precast concrete member
- R_0 = distance of pivot point from center of gravity of the rocking member
- $sign(\theta)$ = sign of angular displacement
- $sign(\dot{\theta})$ = sign of angular velocity
- SH = shore hardness
- t_r = rubber thickness
- \ddot{u}_g = horizontal ground acceleration
- U_g = gravitational potential energy
- U_{PT} = strain energy in the unbonded post-tensioning tendon
- β = dimensionless modeling parameter
- δL = elongation of the unbonded tendon due to the angular displacement of the precast concrete member
- ΔE_{impact} = energy loss per impact
- ζ = equivalent viscous damping ratio
- θ = angular displacement of the rocking member
- θ_o = initial angular displacement of the free vibration motion
- θ_n = amplitude of angular displacement after n impacts
- $\dot{\theta}$ = angular velocity of the precast concrete member
- $\ddot{\theta}$ = angular acceleration of the rocking member
- λ = modeling parameter defining the magnitude of the tendon elongation due to the angular displacement of the precast concrete member

About the authors



Dimitrios Kalliontzis is a former PhD student in the Department of Civil, Environmental, and Geo-Engineering at the University of Minnesota in Minneapolis.



Sri Sritharan is the Wilkinson Chair Professor in the Department of Civil, Construction, and Environmental Engineering at Iowa State University in Ames.

Abstract

The use of precast concrete members with jointed connections for seismic applications has gained momentum recently; however, these systems may have limited application in seismic regions. This is because their dominant mechanism of impact damping is considered to be inadequate to dissipate the seismic energy imparted to them. With no hysteresis elements, precast concrete members with jointed connections may undergo long durations of motion and large lateral drifts when subjected to seismic loads. This paper investigates a method that can allow these members to dissipate the seismic energy efficiently by having them rock on a thin rubber layer that is placed at the jointed connection. Experiments that examine the use of various classes and layer thicknesses of rubber show that this method can improve damping in these members. Using experimental and numerical data, this paper quantifies the energy dissipation and seismic responses associated with this use of rubber. It is shown that rubber layers with high shore hardness of 90 and thickness between 6.35 and 25.4 mm (0.25 and 1 in.) improve the amount of damping in lateral-load-resisting systems using precast concrete members and produce satisfactory seismic response for these systems.

Keywords

Coefficient of restitution, controlled rocking, impact, jointed connection, rubber, unbonded post-tensioning.

Review policy

This paper was reviewed in accordance with the Precast/Prestressed Concrete Institute's peer-review process.

Reader comments

Please address any reader comments to *PCI Journal* editor-in-chief Tom Klemens at tklemens@pci.org or Precast/Prestressed Concrete Institute, c/o *PCI Journal*, 8770 W. Bryn Mawr Ave., Suite 1150, Chicago, IL 60631. [f](#)